ACS APPLIED POLYMER MATERIALS

pubs.acs.org/acsapm Article

Aqueous Assembly and Hydrogel Rheology of Sustainable Glyoxylate-Based Copolymers

Xuechen Yin, David R. O. Hewitt, Bingqian Zheng, Xiaoxi Yu, Amanda J. Carr, Robert B. Grubbs, and Surita R. Bhatia*

Cite This: *ACS Appl. Polym. Mater.* 2022, 4, 5493−5500 Read Online

ACCESS | Metrics & More | Article Recommendations | Supporting Information

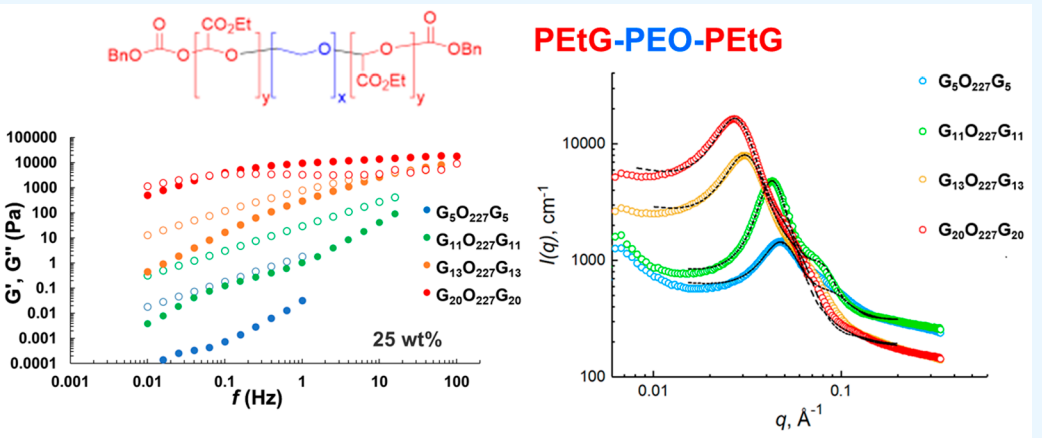

ABSTRACT: The self-assembly of poly(ethyl glyoxylate)−poly(ethylene oxide)−poly(ethyl glyoxylate) (PEtG−PEO−PEtG) triblock copolymers in aqueous environments was systematically studied by using rheology and small-angle neutron scattering (SANS). These systems form associative micellar gels in water, with the PEtG end-blocks forming micelle cores and the PEO mid-blocks forming loops in the micelle coronas and intermicellar bridges. As PEtG block length is increased, rheology shows slower relaxation behavior, consistent with a longer lifetime of intermicellar bridges and associations. The length of the self-immolative PEtG block can be used to tailor the mechanical properties, size of nanoscale hydrophobic domains, and larger-scale assembly behavior of the block copolymer gels. These results can guide the design of self-immolative block copolymers with desirable rheological properties and nanoscale structures for a variety of applications.

KEYWORDS: *glyoxylate, degradable, copolymers, hydrogel, rheology, neutron scattering*

1. INTRODUCTION

Polyaldehyde-based block copolymers have been utilized in self-immolative materials, where characteristic structural changes and degradation take place as a result of exposure to specific stimuli.[1,2] For example, Ribitsch et al. reported amphiphilic poly(phthalaldehyde)−Surfonamine block copolymers with controlled acid-catalyzed degradation behavior.[3] More recently, core−shell micelles of amphiphilic block copolymers with degradable polyaldehyde cores and stabilized shells have been used to formulate hollow nanocapsules for controlled released and nutrient preservation systems.[4,5]

Poly(ethyl glyoxylate) (PEtG), synthesized by using aldehyde polymerization methods, has emerged as one of the popular block components for self-immolative systems,[1,2] in addition to the widely studied polycarbamate- and poly-phthalaldehyde-based systems.[6,7] Earlier studies of polyglyoxylates for industrial applications focused on poly(glyoxylic acid) and poly(methyl glyoxylate).[8,9] PEtG, whose biodegradation and toxicity properties have been systematically evaluated,[10] was subsequently developed as a better alternative for pharmaceutical systems because the final degradation products, ethanol and glyoxylic acid, are biocompatible and biodegradable. Amphiphilic block copolymers with AB and ABA structures consisting of poly(ethylene glycol) (PEG) and PEtG have been prepared by Jo et al. and have been shown to release loaded paclitaxel (PTX) in a pH-dependent manner.[11] However, prior to use of PEtG-based block copolymers in clinical and biomedical applications, determining the rheo-

Received: March 31, 2022
Accepted: June 24, 2022
Published: July 12, 2022

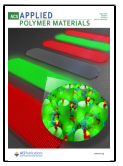

Scheme 1. Synthesis of PEtG−PEOPEtG Triblock Copolymers with Varying PEtG Block Length

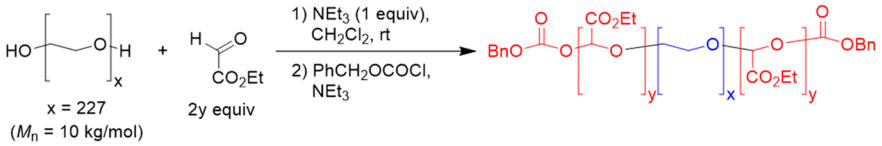

logical properties and nano-/microscale structure of amphiphilic PEtG-related block copolymers is necessary. Gillies and co-workers have reported the synthesis of PEG−PEtG−PEG triblock copolymers with a UV-responsive end-cap. The self-assembly of copolymers into micelles or nanoparticles in aqueous media with controlled depolymerization upon UV irradiation was demonstrated.[12,13] More recently, polymerization and copolymerization of *n*-butyl glyoxylate, L-menthyl glyoxylate, and chloral with ethyl glyoxylate were explored to form UV-light-responsive polyglyoxylate-based diblock copolymers, resulting in systems with tunable self-assembly, drug loading profiles, and toxicity.[14] In each of these examples, the block copolymers are prepared by the coupling of end-functionalized PEG (hydroxy or azide) with telechelic PEtG (isocyanate or alkyne), which limits the polymer architectures that can be prepared to those in which PEtG is not a terminal block. For the preparation of hydrogels, polymer architectures in which terminal hydrophobic PEtG blocks are connected by a hydrophilic PEG block are desirable.

Here we report the viscoelasticity and nanoscale assembly of a series of PEtG−PEO−PEtG triblock copolymers in aqueous media as a function of PEtG block length. We use the designation $G_xO_yG_x$ to refer to samples with end-blocks comprising *x* repeat units of ethyl glyoxylate and mid-blocks of *y* repeat units of ethylene oxide. The rheological properties and nanostructure of these triblock gels were characterized by small-amplitude oscillatory shear (SAOS) rheology and small-angle neutron scattering (SANS), respectively. These results provide a platform for designing materials with tunable viscoelasticity and micelle size to be used in biomedical applications such as drug delivery and tissue engineering.

2. MATERIALS AND METHODS

2.1. Materials. Triethylamine (NEt_3, 99%, Acros Organics), dichloromethane (CH_2Cl_2, 99.9%, Extra Dry, stabilized, AcroSeal, Acros Organics), tetrahydrofuran (THF, Extra-dry, Acros Organics), benzyl chloroformate (50 wt % in toluene, Acros Organics), diethyl ether (98%, ACS grade, Millipore Sigma), and hexanes (≥98.5%, ACS grade, Macron Fine Chemicals) were used without further purification. Ethyl glyoxylate (EtG, 50% solution in toluene, Acros Organics) was distilled over phosphorus pentoxide to remove toluene, doubly distilled over phosphorus pentoxide, and then stored and handled in the glovebox.[12] Methoxybenzyl alcohol (3-MBA, Alfa Aesar) was distilled over calcium hydride and then stored and handled in the glovebox. Poly(ethylene glycol) (PEG, M_n = 10 kg/mol, Alfa Aesar) was subjected to azeotropic distillation with toluene and then dried under vacuum prior to being placed in a nitrogen-filled glovebox.

2.2. Synthesis of PEtG−PEG−PEtG Triblock Copolymer $G_5O_{227}G_5$ (Representative of $G_{11}O_{227}G_{11}$, $G_{13}O_{227}G_{13}$, and $G_{20}O_{227}G_{20}$). In a nitrogen-filled glovebox, PEG (4.0 g, 0.4 mmol) was dissolved in CH_2Cl_2 (10 mL) in a flask equipped with a magnetic stir bar. NEt_3 (56 μL, 0.4 mmol) and EtG (1.0 mL, 10.4 mmol) were added to the reaction flask, and the mixture was allowed to stir at room temperature for 1 h. Benzyl chloroformate (0.682 mL, 2.0 mmol, 50 wt % in toluene) was subsequently added followed by NEt_3 (390 μL, 2.8 mmol, 7.0 equiv). The reaction mixture was left to stir overnight and then was precipitated into hexanes. The precipitant was isolated by decanting the supernatant, redissolving in CH_2Cl_2, and precipitating again in diethyl ether. The final white solid was obtained by vacuum filtration in a fritted funnel After drying in vacuo at 35 °C for 48 h, PEtG−PEG−PEtG was obtained as a white solid (4.63 g, 92.0%). ^{1}H NMR (700 MHz, $CDCl_3$): δ 7.4−7.8 (10H, br, $C_6\mathbf{H}_5-$), 5.5−5.7 (1H per EtG repeating unit, br, $-C\mathbf{H}O-$), 4.2 (2H per EtG repeating unit, br, $-OC\mathbf{H}_2-$), 3.65 (4H per PEO repeating unit, br, $-C\mathbf{H}_2C\mathbf{H}_2O-$), 1.3 (3H per EtG repeating unit, br, $-C\mathbf{H}_3$).

2.3. Preparation of Block Copolymer Solutions and Gels. Each polymer solution or gel was prepared by slowly adding a dried PEtG−PEO−PEtG sample into a fixed weight of solvent while stirring. Magnetic stirring was performed until the polymer sample was fully added and the mixture had appeared homogeneous for at least 1 h. The mixture was subsequently kept in a sealed vial at room temperature for 1 day to ensure equilibrium. Water was used as the solvent for rheological tests while deuterated water (D_2O) was chosen as the solvent for neutron scattering measurements. The concentration of polymer samples was set to be 25 wt % for all the tests.

2.4. Rheological Characterization. Small-amplitude oscillatory shear studies were performed by using a TA Instruments stress-controlled AR-G2 rheometer. The gels were transferred onto the Peltier plate and were trimmed to fit a parallel plate (40 mm) geometry which were used to perform the stress sweeps and frequency sweeps. The gels and geometry were covered by a solvent trap to avoid evaporation of water. Amplitude sweeps were performed before the frequency sweeps to ensure that all experiments were performed within the linear viscoelastic regime. Representative amplitude sweep is shown in Figure S1. All tests were performed at 25 °C.

2.5. SANS Characterization. Neutron scattering measurements were performed at the Center for High Resolution Neutron Scattering (CHRNS) located at National Institute of Standards and Technology (NIST), Gaithersburg, MD. SANS measurements were conducted on the 30 m SANS instrument on beamline NG7, with additional characterization at lower *q* performed on the NG3 beamline on the VSANS instrument (Supporting Information). VSANS is the designation provided by NIST and indicates that this instrument provides a lower range of *q* than a conventional SANS experiment, but it should be noted that this is distinct from the ultrasmall-angle instrument (USANS) on beamline BT5 at NIST. Multiple detector arrays with controlled wavelength resolution allow measurement of various sample environments with a wide *q* range. The *q* range covered in the spectra was 0.007 $Å^{-1} < q < 0.164$ $Å^{-1}$ (0.6−14.3 nm) for NG3 and 0.00144 $Å^{-1} < q < 0.338$ $Å^{-1}$ (3.0−694.4 nm) for NG7. The measurements were performed at 25 °C for all the samples. Data reduction and normalization were performed by using standard techniques, and all neutron scattering data reported here are on an absolute scale except where noted. Scattering length densities (SLD) used in model fittings and calculations are 1.28×10^{-6}, 6.38×10^{-7}, and 6.36×10^{-6} $Å^{-2}$ for PEtG, PEO, and D_2O, respectively. Our experimental design relies on use of a deuterated solvent and the inherent contrast between the solvent and hydrogenated mid-block and end-blocks. As our samples have a large percentage of solvent, this approach minimizes the incoherent background that would be present if a hydrogenated or mixed solvent were used; however, the resulting scattering will be due to both the micelle core and corona, necessitating the use of a more complex model to account for this when fitting the data. An alternative approach would be to use a mixed solvent of H_2O/D_2O to contrast-match one block or another. While this allows one to isolate scattering from either the core or corona, use of a mixed solvent results in a high incoherent background, and a longer experiment time is required to obtain

https://doi.org/10.1021/acsapm.2c00542
ACS Appl. Polym. Mater. 2022, 4, 5493−5500

data with good statistics. Use of a block copolymer with one block selectively deuterated and a deuterated solvent would be ideal, as it would address both these issues. This approach may be pursued in future studies.

3. RESULTS AND DISCUSSION

3.1. Triblock Copolymer Synthesis. PEtG−PEG−PEtG triblock copolymers were prepared by using triethylamine-catalyzed polymerization of ethyl glyoxylate from the hydroxyl end-groups of PEG (Scheme 1).[15] Capping of the low ceiling temperature (T_c = 37 °C) PEtG terminal hemiacetal groups with benzyl chloroformate was done to prevent depolymerization at physiological temperatures.[12,16] Azeotropic distillation of toluene from commercially available PEG was sufficient to allow use of the hygroscopic PEG as a macroinitiator for EtG polymerization. To minimize moisture contamination, polymerization was performed under a nitrogen atmosphere in a glovebox. PEtG−PEG−PEtG copolymers with a range of compositions were prepared to allow examination of the effect of PEtG/PEG ratio on polymer hydrogel properties. PEtG block lengths were somewhat lower than expected based upon stoichiometry and conversion, suggesting residual water concentrations in the polymerization mixtures ranging from 20 to 37 mM. The characteristics of triblock copolymers synthesized are listed in Table 1. ^{1}H NMR spectra of crude and isolated PEtG−PEO−PEtG triblock copolymers are shown in Figures S2−S9.

Table 1. Characteristics of PEtG−PEO−PEtG Triblock Copolymers Synthesized[a]

sample	$Đ$[b]	$[M]_0/[I]_0$	EtG conv (%)[c]	M_n^{NMR} (kg/mol)[d]
$G_5O_{227}G_5$	1.22	26	74	11.3
$G_{11}O_{227}G_{11}$	1.23	50	78	12.5
$G_{13}O_{227}G_{13}$	1.21	76	81	12.9
$G_{20}O_{227}G_{20}$	1.23	100	81	14.4

[a]PEO (10 kg/mol), NEt_3 (0.5 equiv), CH_2Cl_2 (10 mL), 60 min, room temperature. End-capped with benzyl chloroformate (2.5 equiv). [b]Dispersity ($Đ = M_w/M_n$) estimated by SEC vs PS standards (Figure S10). [c]Ethyl glyoxylate conversion estimated by ^{1}H NMR analysis of crude polymerization mixture by comparison of the area of the EtG−OCH_2− methylene peak (4.4 ppm) with the area of the PEtG methylene peak (4.2 ppm) (Figures S2−S5). [d]M_n estimated after precipitation by ^{1}H NMR by comparison of the integrated area of the PEO methylene peak at 3.65 ppm (br, 4**H** per PEO repeating unit, $-CH_2CH_2O-$) to the proton-weighted average of the integrated areas of PEtG proton peaks at 5.30−5.60 ppm (1H per repeating unit, $-CHRO-$), 4.23 ppm (2H per repeating unit, $-OCH_2-$), and 1.30 ppm (3H per repeating unit, $-CH_3$) (Figures S6−S9).

3.2. Rheological Studies. Storage moduli and loss moduli for PEtG−PEO−PEtG triblock gels and solutions are shown in Figure 1a. Data points at higher frequencies where the raw phase was above 150° are not shown because of concerns with instrument inertia. All the copolymer systems behave as viscoelastic liquids with loss moduli that are higher than the storage moduli at low frequency. As the frequency is increased for $G_{20}O_{227}G_{20}$ and $G_{13}O_{227}G_{13}$, G' exceeds G'' at higher frequencies, and the sample's elastic response becomes stronger. Crossover points where the G' curves intersect with the G'' profiles can be observed for $G_{20}O_{227}G_{20}$ and $G_{13}O_{227}G_{13}$. With larger PEtG block lengths, the crossover points occur at a lower frequency, indicative of longer relaxation times ($\tau \sim 1/f_{crossover}$) in the associative network.

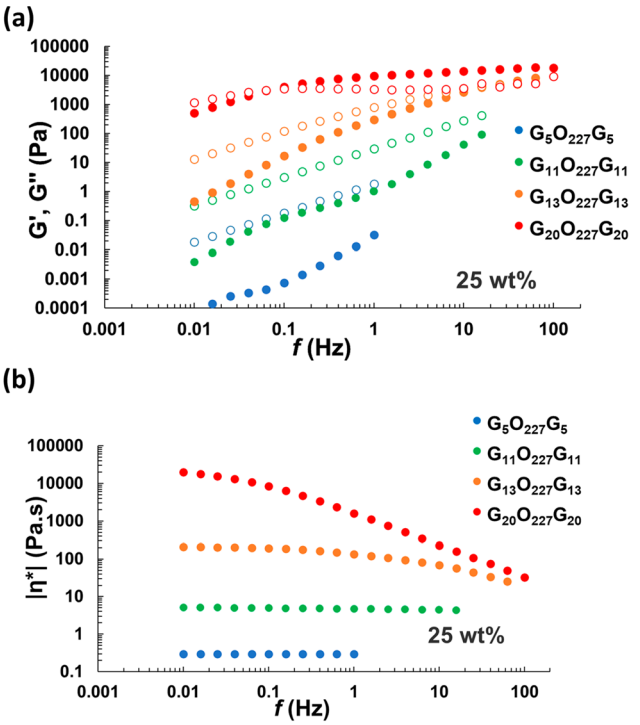

Figure 1. (a) Storage moduli (G', filled symbols) and loss moduli (G'', open symbols) and (b) complex viscosity $|\eta^*|$ in frequency sweeps of PEtG−PEO−PEtG triblock copolymers hydrogels with increasing PEtG block length at 25 wt %.

The relaxation times calculated for $G_{20}O_{227}G_{20}$ and $G_{13}O_{227}G_{13}$ are about 2.5 and 0.01 s, respectively. This change in the PEtG block length size results in an increase of the relaxation time of 2 orders of magnitude. The storage moduli for this series of copolymers (Figure 1a) show a pronounced enhancement of elasticity, characterized by an increase of G', for copolymers with higher degree of polymerization (DP) of the PEtG block segment. Over most of the frequency range, we observe an increase in the storage moduli as the PEtG block length is increased. This trend is expected and has been seen in other associative polymer solutions and gels.[17,18] For example, Kornfield and co-workers have reported the rheology of gels of PEGs terminated at both ends with fluoroalkyl segments and find that as the fluoroalkyl chain length is increased there is an increase in G'.[17] Comparison of the $G_{11}O_{227}G_{11}$ and $G_{13}O_{227}G_{13}$ is particularly interesting; we observe a significant increase in G' at lower frequencies even with a small change in block length. Pham et al. also observed a significant increase in the high-frequency storage modulus, G'_∞, of associative polymer networks of PEO chains with C16 and C18 alkyl end-groups,[19] with the C18 systems displaying a G'_∞ up to 130% greater than the C16 systems. Although this effect may not be expected on the basis of classic theories of transient networks that attribute elasticity only to the mid-blocks that bridge micelles, the authors show that their results are consistent with the scaling theory of Semenov et al.[20] for associative polymer micelles, which accounts for contributions to the elasticity of both bridging polymer chains and compression of micelles. The expression for G'_∞ in this model includes the micelle aggregation number N_{agg}, which is typically very sensitive to the length of the hydrophobic end-block; this can be verified for our copolymers through SANS, discussed in detail below. Thus, it is likely that the change in

https://doi.org/10.1021/acsapm.2c00542
ACS Appl. Polym. Mater. 2022, 4, 5493−5500

storage moduli that we observe is also due in part to compression of micelles, similar to the findings of Pham et al.[19] As the DP of the PEtG end-blocks are increased by 12−13 units, G' increases by roughly 2 orders of magnitude at 0.1 Hz and slightly above 1 order of magnitude at 1.0 Hz.

In addition to other material viscoelastic functions, the complex viscosity (η^*) is often used to evaluate the rheological behavior of block copolymer gels and solutions because of its high sensitivity to structural rearrangement during fractal gel formation.[21] The frequency-dependent complex viscosity $|\eta^*|$ is given by[22]

$$|\eta^*| = \frac{\sqrt{G'^2 + G''^2}}{2\pi f} = \frac{|G^*|}{2\pi f}$$

where G^* is the frequency-dependent complex modulus. Although the complex viscosity is directly related to the viscoelastic moduli presented above, plotting the data in this way can sometimes yield insight into possible structural change; for example, upturns may be observed at high frequency if structural reorganization takes place during oscillatory shear.[23] The complex viscosity of this series of copolymers at 25 wt % in water is shown in Figure 1b. There is no apparent upturn at higher frequency of the complex viscosity for each copolymer gel solution, which is consistent with what we would expect given the profiles of the viscoelastic moduli. In addition, the liquidlike behaviors of $G_5O_{227}G_5$ and $G_{11}O_{227}G_{11}$ acquired from moduli analysis are further verified by constant $|\eta^*|$ values over the measurable frequency range.[24] For $G_{13}O_{227}G_{13}$ and $G_{20}O_{227}G_{20}$, the systems show a decrease in the complex viscosity at higher frequencies. Although we did not measure the viscosity under in a steady shear field, these systems will likely display shear-thinning behavior (which typically occurs at shear rates above $1/f_{crossover}$),[25] which can be useful for injectable materials used in tissue regeneration,[26,27] drug delivery,[28,29] and cell encapsulation.[30,31] As above, the difference between the $G_{11}O_{227}G_{11}$ and $G_{13}O_{227}G_{13}$ copolymers is striking; we observe an increase of more than an order of magnitude in $|\eta^*|$ with a very small change in the end-block length. Again, this is consistent with observations of Pham et al., who found an increase of nearly 2 orders of magnitude in the low-shear viscosity of associative networks of PEO chains capped with C16 alkyl groups as compared to C18 groups,[19] again suggesting that micellar compression and micelle structure are important contributions to the rheological behavior of these systems. By tuning the hydrophobic PEtG block length in PEtG−PEO−PEtG copolymer gel solutions, we can simultaneously control the rheological properties and relaxation time. The optimization of these physical properties is important for injectable hydrogel applications, which require viscous flow under shear stress (shear-thinning) and time-dependent modulus recovery upon relaxation (self-healing).[32]

3.3. SANS Analysis. To probe the nanoscale structure, small-angle neutron scattering (SANS) was performed (Figure 2). Small-angle scattering has been widely utilized to study the multiscale organization of polymers with varying block content.[33] A core−shell ellipsoid form factor model was utilized to fit the scattering spectra, with a hard-sphere structure factor to account for interparticle interactions. Correlation peaks appear in all of samples, indicating liquidlike ordering of micelles within the gels and solutions. The micellar spacing, given by $d = 2\pi/q$, is calculated and shown in Table 2. Calculated micellar spacing is the most probable distance between the center of PEtG micelles. The micellar domain spacing shows a systematic increase from 129 to 234 Å with increasing hydrophobic PEtG block length. The clear trend obtained indicates that the slight variation of peak position within each sample can be neglected. The correlation peaks are also observed for all of these samples at the same concentration studied by VSANS (Figure S11). The d-spacing values obtained are fairly comparable to that in SANS profiles, establishing our confidence in the precision of intermicellar spacing. With larger PEtG block, hydrophobic micellar cores are expected to grow, leading to a larger d-spacing. The increase in micelle aggregation number, expansion of PEtG domains, and potential increase in intermicellar bridging interactions all likely contribute to the enhancement of the storage modulus with increasing PEtG block. In addition, there is an upturn for each sample at low q. This behavior is often attributed to increases in the intermicellar attraction, as the value of the structure factor at low q is related to the osmotic compressibility. Interestingly, for our samples, this increase is more pronounced for the samples with smaller PEtG blocks, suggesting that other factors may be influencing the excess scattering at low q. Our VSANS results (Figure S11) suggest formation of large-scale structure in some samples, which has also been observed for associative hydrogels of ABA block copolymers with poly(lactic acid) (PLA) end-blocks, PLA−PEO−PLA.[34] If such large structures are present, this would complicate interpretation of the low q scattering, as it would not solely be due to intermicellar attraction.

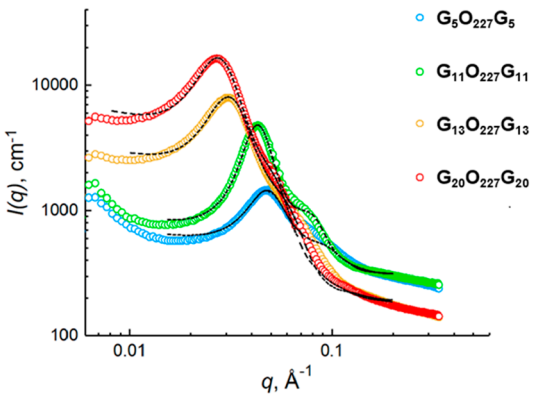

Figure 2. SANS spectra of PEtG−PEO−PEtG copolymer gel solution with varied PEtG block length at 25 wt %. Dashed lines are best fits to the core−shell ellipsoid model with hard-sphere structure factor. Fits were performed with data in absolute units; data and fits have been vertically shifted here for clarity.

Table 2. Calculated d-Spacing from Correlation Peaks in SANS Profiles[a]

	d-spacing (Å)	
sample	NG7−SANS	NG3−VSANS
$G_5O_{227}G_5$	129 ± 14	129 ± 13
$G_{11}O_{227}G_{11}$	147 ± 16	144 ± 14
$G_{13}O_{227}G_{13}$	204 ± 22	209 ± 21
$G_{20}O_{227}G_{20}$	234 ± 26	233 ± 23

[a]Uncertainties are estimated based on the instrument resolution.

3.4. Core−Shell Model Fits to Scattering Data. After attempting to fit the data with several types of models, we selected a core−shell ellipsoidal micelle model for the form factor and a Percus−Yevick hard-sphere structure factor. As is

https://doi.org/10.1021/acsapm.2c00542
ACS Appl. Polym. Mater. 2022, 4, 5493−5500

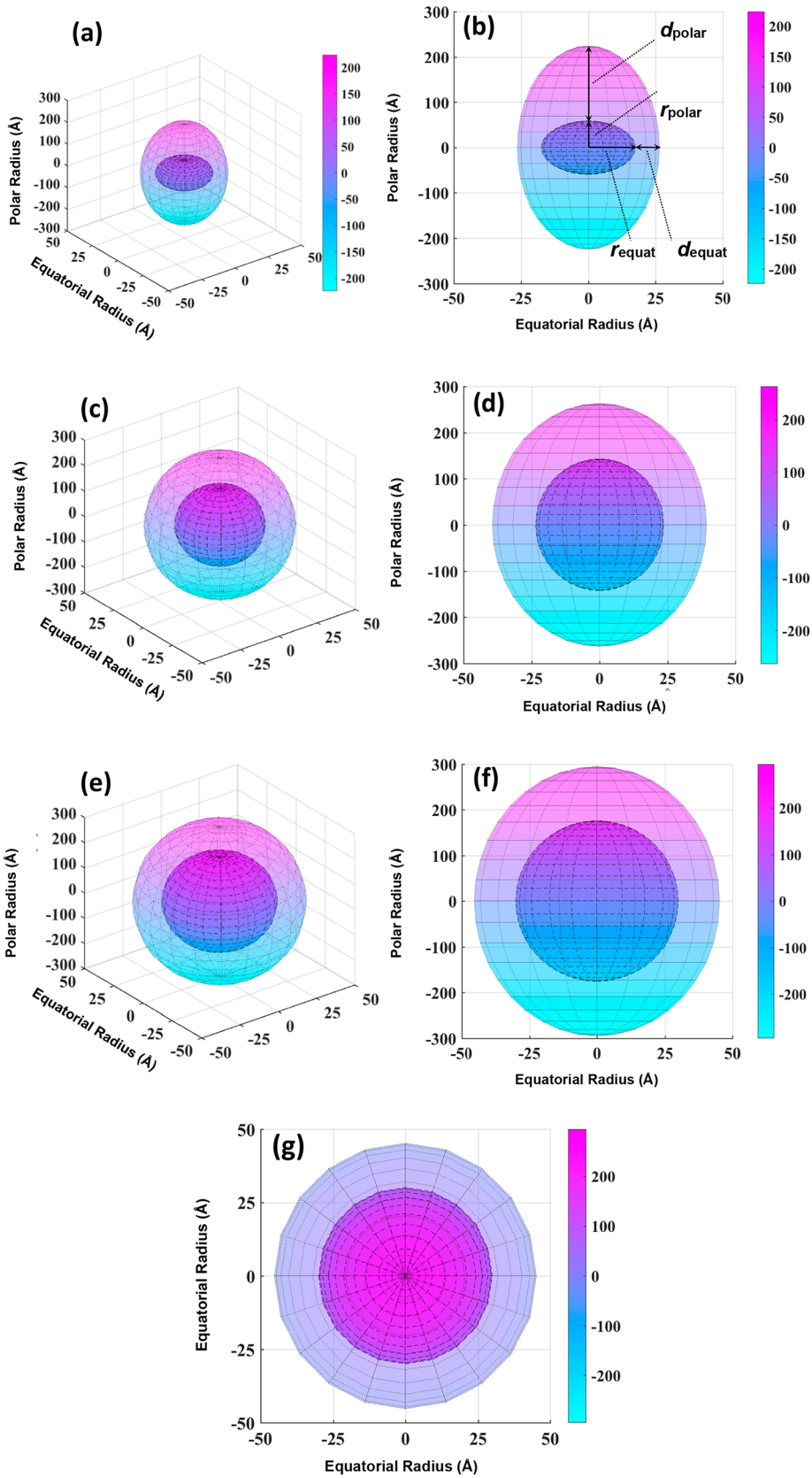

Figure 3. Depiction of the core−shell ellipsoid structure of PEtG−PEO−PEtG copolymer gel solutions in three-dimensional space. (a, c, e) 3D view of $G_{11}O_{227}G_{11}$, $G_{13}O_{227}G_{13}$, and $G_{20}O_{227}G_{20}$. (b, d, f) X−Z plane cross section of $G_{11}O_{227}G_{11}$, $G_{13}O_{227}G_{13}$, and $G_{20}O_{227}G_{20}$. (g) X−Y plane view of $G_{20}O_{227}G_{20}$.

https://doi.org/10.1021/acsapm.2c00542
ACS Appl. Polym. Mater. 2022, 4, 5493−5500

often the case with scattering data, multiple models may provide a reasonable fit to the data. However, results from the core−shell ellipsoidal model are presented as this model captured several qualitative features of the SANS data and resulted in low values for the residuals, indicating goodness of fit, and low uncertainties in the fit parameters. We did not see any evidence of long-range order in the form of higher-order peaks in our data. The diagram describing the geometric parameters in core−shell ellipsoid form factor is shown in Figure 3. The equatorial radius of the core and thickness of shell at the equator are given by r_{equat} and d_{equat}, respectively, with $R_{equat} = r_{equat} + d_{equat}$ being the equatorial radius of the micelle. Likewise, r_{polar} is the polar radius of core while d_{polar} indicates the polar thickness of shell, with $R_{polar} = r_{polar} + d_{polar}$ being the polar radius of the micelle. The axial ratio of the core, x_{core}, given as r_{polar}/r_{equat}, can further describe the circular symmetry in the ellipsoid. The parameter x_{core} is always larger than 1 for PEtG−PEO−PEtG systems where the core is a prolate ellipsoid. Oblate ellipsoids and spherical cores are obtained when $x_{core} < 1$ and $x_{core} = 1$, respectively.

For the equation applied in the model, the overall scattering intensity is calculated as

$$I(q) = \frac{\text{scale}}{V} P^2(q, \alpha) + \text{background}$$

where the normalized form factor is given by

$$P(q, \alpha) = p(q, r_{equat}, r_{polar}, \alpha) + p(q, R_{equat}, R_{polar}, \alpha)$$

and

$$p(q, r_{equat}, r_{polar}, \alpha) = 3\Delta\rho_1 V \times \frac{\{\sin[qm(r_{equat}, r_{polar}, \alpha)] - \cos[qm(r_{equat}, r_{polar}, \alpha)]\}}{[qm(r_{equat}, r_{polar}, \alpha)]^3}$$

$$p(q, R_{equat}, R_{polar}, \alpha) = 3\Delta\rho_2 V \times \frac{\{\sin[qm(R_{equat}, R_{polar}, \alpha)] - \cos[qm(R_{equat}, R_{polar}, \alpha)]\}}{[qm(R_{equat}, R_{polar}, \alpha)]^3}$$

and

$$m(r_{equat}, r_{polar}, \alpha) = (r_{equat}^2 \sin^2\alpha + r_{polar}^2 \cos^2\alpha)^{0.5}$$

$$m(R_{equat}, R_{polar}, \alpha) = (R_{equat}^2 \sin^2\alpha + R_{polar}^2 \cos^2\alpha)^{0.5}$$

Here V is the volume of the ellipsoid; the $\Delta\rho$ terms are the relevant scattering length density contrast, either $\rho_{core} - \rho_{shell}$ or $\rho_{shell} - \rho_{solvent}$; and α is the angle between the axis of the ellipsoidal structure and scattering vector. Polydispersity (Σ) with a Schulz distribution function in the equatorial size of micellar core was introduced in the model fitting to effectively describe the micelle sizes.

Structural parameters of PEtG−PEO−PEtG micelle systems obtained from the fits to core−shell ellipsoid model are presented in Table 3. Visualized diagrams of core−shell ellipsoidal micelles obtained in Matlab are presented in Figure 3. Moderate polydispersity (Σ = 0.25−0.35) and a Percus−Yevick hard-sphere structure factor are successfully applied to optimize the fitting profiles in terms of correlation peaks and mid-q scatterings. The volume fraction of hard spheres (φ_i) is thus generated to describe the nonoverlapping region occupied by hard spheres. From the perspective of the $X-Y$ plane, an increase of both the core and micelle with larger PEtG block is observed. The equatorial and polar semiaxis length both display a steady increase for the core and micelle as PEtG length is increased. The aggregation number N_{agg} can then be calculated to describe the number of PEtG chains forming the micellar core via hydrophobic interaction:

$$N_{agg} = \frac{4\pi r_{equat}^2 r_{polar}}{3V_{PEtG}}$$

where V_{PEtG} is the molecular volume of PEtG. N_{agg} was found to increase from 18 to 75 as the PEtG block length was increased. A similar trend of larger aggregation number with increasing hydrophobic blocks has been found in other studies of block copolymers in selective solvents.[17,18] As discussed above, if the storage modulus of these systems can be attributed to both bridging mid-block chains and compression of the micelle corona, the increase in N_{agg} from 18 for $G_{11}O_{227}G_{11}$ to 59 for $G_{13}O_{227}G_{13}$ is consistent with the increase in storage modulus that we observe between these two copolymers.

The dimensions of the PEO shell do not strongly vary with PEtG block length. This may be expected for this series of copolymers, as the block length of PEO is held constant. However, because the overall size of the micelle increases with PEtG block length, the volume of the shell region, calculated as $V_{shell} = V_{micelle} - V_{core}$, does expand from $G_{11}O_{227}G_{11}$ to $G_{20}O_{227}G_{20}$. The change in V_{shell} impacts the degree of hydration, a parameter sometimes used to characterize the configuration of chains in the micelle shell, which can be important in describing interactions of polymeric micelles with biomolecules and cells, for example, impacting the adsorption of biomolecules during delivery applications and bioimaging applications.[35,36] The degree of hydration (φ_{PEO}) can be expressed as[37]

$$\varphi_{PEO} = 1 - \frac{3N_{agg}V_{PEO}}{4\pi(R_{equat}^2 R_{polar} - r_{equat}^2 r_{polar})}$$

Table 3. Fitting Parameters of Core−Shell Ellipsoid Model for PEtG−PEO−PEtG Systems with Different PEtG Block Lengths at 25 wt %

parameter		$G_{11}O_{227}G_{11}$	$G_{13}O_{227}G_{13}$	$G_{20}O_{227}G_{20}$
core	r_{equat} (Å)	17.5 ± 0.3	23.5 ± 0.1	30.1 ± 0.3
	x_{core}	3.36 ± 0.20	6.06 ± 0.01	5.86 ± 0.50
	r_{polar} (Å)	58.8 ± 4.6	142.4 ± 0.9	176.4 ± 16.9
shell	d_{equat} (Å)	9.0 ± 0.4	15.9 ± 0.1	15.2 ± 0.6
	x_{shell}	18.31 ± 0.91	7.59 ± 0.02	7.80 ± 0.79
	d_{polar} (Å)	164.8 ± 15.9	120.7 ± 1.1	118.6 ± 17.1
micelle	R_{equat} (Å)	26.5 ± 0.7	39.4 ± 0.2	45.3 ± 1.0
	R_{polar} (Å)	223.6 ± 20.5	263.1 ± 2.0	295.0 ± 34.0
Σ		0.25	0.25	0.35
φ_i		0.408	0.314	0.324
N_{agg}		18	59	75
φ_{PEO}		0.58	0.42	0.44
S_{c-s}/N_{agg} (nm^2)		5.8	5.7	7.1
S_{s-w}/N_{agg} (nm^2)		32.8	17.5	17.8

https://doi.org/10.1021/acsapm.2c00542
ACS Appl. Polym. Mater. 2022, 4, 5493−5500

Here V_{PEO} is the molecular volume of PEO. As the hydrophobic PEtG blocks increase, the degree of hydration first decreases and then remains nearly constant. Initially, the PEO chains in EtG-50 adopt a comparatively more stretched conformation to approach the PEO in neighboring micelles and enhance the intermicellar interaction. In $G_{13}O_{227}G_{13}$ and $G_{20}O_{227}G_{20}$, PEO chains then tend to contract and form a more clustered or collapsed configuration, possibly driven by crowding of chains with the high micelle aggregation number. The surface area per PEO chain at the core−shell interface and outer shell surface is expressed as S_{c-s}/N_{agg} and S_{s-w}/N_{agg}, respectively. Davis has reported the surface area per PEG chain in PLA−PEG assemblies varies between 1.9−7.8 and 12−23 nm^2 for the core/shell and shell/solvent interface, respectively.[38] These are comparable to the surface area per PEO chain in PEtG−PEO−PEtG systems we obtain for corresponding interfaces. The contrast between surface area per PEO chain at the core−shell interface and at the periphery of the shell first diminishes markedly and then slightly decreases with increasing the PEtG block length from $G_{11}O_{227}G_{11}$ to $G_{20}O_{227}G_{20}$. This again implies that for $G_5O_{227}G_5$, where the MW of PEtG is lower, the PEO chains with higher surface area per chain at shell/solvent interface are favored to stretch outward. By contrast, the PEO chains in $G_{13}O_{227}G_{13}$ and $G_{20}O_{227}G_{20}$ adopt a more coiled conformation as a result of having a smaller S_{s-w}/N_{agg}.

4. CONCLUSIONS

A series of PEtG−PEO−PEtG triblock copolymers were synthesized with a range of DP of the PEtG end-blocks. Larger storage moduli and slower relaxation behavior (longer relaxation times) were observed with increasing PEtG block length, indicating the heightening contribution of hydrophobic interaction of PEtG block to elasticity. SANS patterns show correlation peaks indicative of intermicellar interaction, which shift toward lower scattering vectors with higher molecular weight of PEtG block, corresponding to a larger spacing between neighboring micelles. SANS data were fit well with a core−shell ellipsoid form factor model with a hard-sphere structure factor. Our results provide a platform for the design and modification of self-immolative block copolymers with tunable rheological properties and nanoscale self-assembly.

■ ASSOCIATED CONTENT

Supporting Information

The Supporting Information is available free of charge at https://pubs.acs.org/doi/10.1021/acsapm.2c00542.

Representative oscillation amplitude sweep of PEtG−PEO−PEtG triblock copolymer $G_{13}O_{227}G_{13}$, ^1H NMR spectra of PEtG−PEO−PEtG triblock copolymers, methods for SEC characterization and SEC traces, data from VSANS experiments and discussion of VSANS data (PDF)

■ AUTHOR INFORMATION

Corresponding Author

Surita R. Bhatia − *Department of Chemistry, Stony Brook University, Stony Brook, New York 11794, United States;* orcid.org/0000-0002-5950-193X; Email: Surita.bhatia@stonybrook.edu

Authors

Xuechen Yin − *Department of Chemistry, Stony Brook University, Stony Brook, New York 11794, United States*

David R. O. Hewitt − *Department of Chemistry, Stony Brook University, Stony Brook, New York 11794, United States*

Bingqian Zheng − *Department of Chemistry, Stony Brook University, Stony Brook, New York 11794, United States*

Xiaoxi Yu − *Department of Chemistry, Stony Brook University, Stony Brook, New York 11794, United States;* orcid.org/0000-0002-9193-9616

Amanda J. Carr − *Department of Chemistry, Stony Brook University, Stony Brook, New York 11794, United States;* orcid.org/0000-0002-8224-7677

Robert B. Grubbs − *Department of Chemistry, Stony Brook University, Stony Brook, New York 11794, United States;* orcid.org/0000-0002-3698-3614

Complete contact information is available at: https://pubs.acs.org/10.1021/acsapm.2c00542

Notes

The authors declare no competing financial interest.

■ ACKNOWLEDGMENTS

The authors gratefully acknowledge financial support from NSF Awards CBET-1335787, DMR-1905547, and CHE-1358959; ACS PRF Grant 55729-ND9; a Turner Dissertation Fellowship for D.R.O.H.; and a Department of Education GAANN Fellowship (Award P200A160163) for B.Z. This research used resources of neutron facilities at the National Institute of Standards and Technology, U.S. Department of Commerce. This research work benefited from the use of the SasView application, originally developed under NSF Award DMR-0520547. SasView contains code developed with funding from the European Union's Horizon 2020 research and innovation program under the SINE2020 project, Grant Agreement No. 654000.

■ REFERENCES

(1) Yardley, R. E.; Kenaree, A. R.; Gillies, E. R. Triggering Depolymerization: Progress and Opportunities for Self-Immolative Polymers. *Macromolecules* **2019**, *52*, 6342−6360.

(2) Sirianni, Q. E. A.; Kenaree, A. R.; Gillies, E. R. Polyglyoxylamides: Tuning Structure and Properties of Self-Immolative Polymers. *Macromolecules* **2019**, *52*, 262−270.

(3) Kostler, S.; Zechner, B.; Trathnigg, B.; Fasl, H.; Kern, W.; Ribitsch, V. Amphiphilic Block Copolymers Containing Thermally Degradable Poly(phthalaldehyde) Blocks. *J. Polym. Sci. Pol Chem.* **2009**, *47*, 1499−1509.

(4) Esser-Kahn, A. P.; Odom, S. A.; Sottos, N. R.; White, S. R.; Moore, J. S. Triggered Release from Polymer Capsules. *Macromolecules* **2011**, *44*, 5539−5553.

(5) Kostler, S. Polyaldehydes: homopolymers, block copolymers and promising applications. *Polym. Int.* **2012**, *61*, 1221−1227.

(6) Sagi, A.; Weinstain, R.; Karton, N.; Shabat, D. Self-immolative polymers. *J. Am. Chem. Soc.* **2008**, *130*, 5434−5435.

(7) Feinberg, A. M.; Hernandez, H. L.; Plantz, C. L.; Mejia, E. B.; Sottos, N. R.; White, S. R.; Moore, J. S. Cyclic Poly(phthalaldehyde): Thermoforming a Bulk Transient Material. *ACS Macro Lett.* **2018**, *7*, 47−52.

(8) Gledhill, W. E.; Saeger, V. W. Degradation of Sodium Polyglyoxylate, a Nonpersistent Metal Sequestrant, in Laboratory Ecosystems. *J. Ind. Microbiol* **1987**, *2*, 97−105.

(9) Vaugelade, C.; Rohmer, A. C.; Burel, F.; Belleney, J.; Duclos, R.; Bunel, C. Progesterone freeze-dried systems in sublingual dosage form. *Int. J. Pharmaceut* **2001**, *229*, 67−73.

(10) Bellonclе, B.; Bunel, C.; Menu-Bouaouiche, L.; Lesouhaitier, O.; Burel, F. Study of the Degradation of Poly(ethyl glyoxylate): Biodegradation, Toxicity and Ecotoxicity Assays. *J. Polym. Environ* **2012**, *20*, 726−731.
(11) Kim, J. K.; Garripelli, V. K.; Jeong, U. H.; Park, J. S.; Repka, M. A.; Jo, S. Novel pH-sensitive polyacetal-based block copolymers for controlled drug delivery. *Int. J. Pharmaceut* **2010**, *401*, 79−86.
(12) Fan, B.; Trant, J. F.; Wong, A. D.; Gillies, E. R. Polyglyoxylates: A Versatile Class of Triggerable Self-Immolative Polymers from Readily Accessible Monomers. *J. Am. Chem. Soc.* **2014**, *136*, 10116−10123.
(13) Fan, B.; Gillies, E. R. Poly(ethyl glyoxylate)-Poly(ethylene oxide) Nanoparticles: Stimuli-Responsive Drug Release via End-to-End Polyglyoxylate Depolymerization. *Mol. Pharmaceut* **2017**, *14*, 2548−2559.
(14) Fan, B.; Yardley, R. E.; Trant, J. F.; Borecki, A.; Gillies, E. R. Tuning the hydrophobic cores of self-immolative polyglyoxylate assemblies. *Polym. Chem-Uk* **2018**, *9*, 2601−2610.
(15) Hewitt, D. R. O.; Grubbs, R. B. Amine-Catalyzed Chain Polymerization of Ethyl Glyoxylate from Alcohol and Thiol Initiators. *ACS Macro Lett.* **2021**, *10*, 370−374.
(16) Kaitz, J. A.; Moore, J. S. Copolymerization of o-Phthalaldehyde and Ethyl Glyoxylate: Cyclic Macromolecules with Alternating Sequence and Tunable Thermal Properties. *Macromolecules* **2014**, *47*, 5509−5513.
(17) Tae, G. Y.; Kornfield, J. A.; Hubbell, J. A.; Lal, J. S. Ordering transitions of fluoroalkyl-ended poly(ethylene glycol): Rheology and SANS. *Macromolecules* **2002**, *35*, 4448−4457.
(18) Aamer, K. A.; Sardinha, H.; Bhatia, S. R.; Tew, G. N. Rheological studies of PLLA-PEO-PLLA triblock copolymer hydrogels. *Biomaterials* **2004**, *25*, 1087−1093.
(19) Pham, Q.; Russel, W.; Thibeault, J.; Lau, W. Micellar solutions of associative triblock copolymers: The relationship between structure and rheology. *Macromolecules* **1999**, *32*, 5139−5146.
(20) Semenov, A.; Joanny, J.-F.; Khokhlov, A. Associating polymers: equilibrium and linear viscoelasticity. *Macromolecules* **1995**, *28*, 1066−1075.
(21) Takenaka, M.; Kobayashi, T.; Hashimoto, T.; Takahashi, M. Time evolution of dynamic shear moduli in a physical gelation process of 1,3:2,4-bis-O-(p-methylbenzylidene)-D-sorbitol in polystyrene melt: Critical exponent and gel strength. *Phys. Rev. E* **2002**, *65*, 041401.
(22) Freytes, D. O.; Martin, J.; Velankar, S. S.; Lee, A. S.; Badylak, S. F. Preparation and rheological characterization of a gel form of the porcine urinary bladder matrix. *Biomaterials* **2008**, *29*, 1630−1637.
(23) Wang, J.; Feng, Y.; Agrawal, N. R.; Raghavan, S. R. Wormlike micelles versus water-soluble polymers as rheology-modifiers: similarities and differences. *Phys. Chem. Chem. Phys.* **2017**, *19*, 24458−24466.
(24) Lopez-Barron, C. R.; Chen, R.; Wagner, N. J.; Beltramo, P. J. Self-Assembly of Pluronic F127 Diacrylate in Ethylammonium Nitrate: Structure, Rheology, and Ionic Conductivity before and after Photo-Cross-Linking. *Macromolecules* **2016**, *49*, 5179−5189.
(25) Xu, X.; Chen, J.; An, L. Shear thinning behavior of linear polymer melts under shear flow via nonequilibrium molecular dynamics. *J. Chem. Phys.* **2014**, *140*, 174902.
(26) Li, Y.; Fan, L. K.; Liu, S. Y.; Liu, W. J.; Zhang, H.; Zhou, T.; Wu, D.; Yang, P.; Shen, L. J.; Chen, J. H.; Jin, Y. The promotion of bone regeneration through positive regulation of angiogenic-osteogenic coupling using microRNA-26a. *Biomaterials* **2013**, *34*, 5048−5058.
(27) Steele, A. N.; Stapleton, L. M.; Farry, J. M.; Lucian, H. J.; Paulsen, M. J.; Eskandari, A.; Hironaka, C. E.; Thakore, A. D.; Wang, H.; Yu, A. C.; Chan, D.; Appel, E. A.; Woo, Y. J. A Biocompatible Therapeutic Catheter-Deliverable Hydrogel for In Situ Tissue Engineering. *Adv. Healthc Mater.* **2019**, *8*, 1801147.
(28) Chen, M. H.; Wang, L. L.; Chung, J. J.; Kim, Y. H.; Atluri, P.; Burdick, J. A. Methods To Assess Shear-Thinning Hydrogels for Application As Injectable Biomaterials. *Acs Biomater Sci. Eng.* **2017**, *3*, 3146−3160.
(29) Purcell, B. P.; Lobb, D.; Charati, M. B.; Dorsey, S. M.; Wade, R. J.; Zellars, K. N.; Doviak, H.; Pettaway, S.; Logdon, C. B.; Shuman, J. A.; Freels, P. D.; Gorman, J. H.; Gorman, R. C.; Spinale, F. G.; Burdick, J. A. Injectable and bioresponsive hydrogels for on-demand matrix metalloproteinase inhibition. *Nat. Mater.* **2014**, *13*, 653−661.
(30) Thakur, A.; Jaiswal, M. K.; Peak, C. W.; Carrow, J. K.; Gentry, J.; Dolatshahi-Pirouz, A.; Gaharwar, A. K. Injectable shear-thinning nanoengineered hydrogels for stem cell delivery. *Nanoscale* **2016**, *8*, 12362−12372.
(31) Alarcin, E.; Lee, T. Y.; Karuthedom, S.; Mohammadi, M.; Brennan, M. A.; Lee, D. H.; Marrella, A.; Zhang, J.; Syla, D.; Zhang, Y. S.; Khademhosseini, A.; Jang, H. L. Injectable shear-thinning hydrogels for delivering osteogenic and angiogenic cells and growth factors. *Biomater Sci-Uk* **2018**, *6*, 1604−1615.
(32) Guvendiren, M.; Lu, H. D.; Burdick, J. A. Shear-thinning hydrogels for biomedical applications. *Soft Matter* **2012**, *8*, 260−272.
(33) Baeza, G. P.; Sharma, A.; Louhichi, A.; Imperiali, L.; Appel, W. P. J.; Fitié, C. F. C.; Lettinga, M. P.; Van Ruymbeke, E.; Vlassopoulos, D. Multiscale organization of thermoplastic elastomers with varying content of hard segments. *Polymer* **2016**, *107*, 89−101.
(34) Yin, X.; Hewitt, D. R. O.; Zheng, B.; Quah, S. P.; Stanley, C. B.; Grubbs, R. B.; Bhatia, S. R. Effect of stereochemistry on nanoscale assembly of ABA triblock copolymers with crystallizable blocks. *Polymer* **2021**, *223*, 123683.
(35) Gon, S.; Kumar, K. N.; Nusslein, K.; Santore, M. M. How Bacteria Adhere to Brushy PEG Surfaces: Clinging to Flaws and Compressing the Brush. *Macromolecules* **2012**, *45*, 8373−8381.
(36) Jokerst, J. V.; Lobovkina, T.; Zare, R. N.; Gambhir, S. S. Nanoparticle PEGylation for imaging and therapy. *Nanomedicine-Uk* **2011**, *6*, 715−728.
(37) Goldmints, I.; vonGottberg, F. K.; Smith, K. A.; Hatton, T. A. Small-angle neutron scattering study of PEO-PPO-PEO micelle structure in the unimer-to-micelle transition region. *Langmuir* **1997**, *13*, 3659−3664.
(38) Riley, T.; Heald, C. R.; Stolnik, S.; Garnett, M. C.; Illum, L.; Davis, S. S.; King, S. M.; Heenan, R. K.; Purkiss, S. C.; Barlow, R. J.; Gellert, P. R.; Washington, C. Core-shell structure of PLA-PEG nanoparticles used for drug delivery. *Langmuir* **2003**, *19*, 8428−8435.

https://doi.org/10.1021/acsapm.2c00542
ACS Appl. Polym. Mater. 2022, 4, 5493−5500